Applied Surface Science 572 (2022) 151371

Contents lists available at ScienceDirect

Applied Surface Science

journal homepage: www.elsevier.com/locate/apsusc

Full Length Article

High-efficiency-and-quality nanostructuring of molybdenum surfaces by orthogonally polarized blue femtosecond lasers

Bo Zhao [a,b], Xin Zheng [a], Yuhao Lei [a], Hongbo Xie [a], Tingting Zou [a], Gan Yuan [a], Wei Xin [c], Jianjun Yang [a,*]

[a] State Key Laboratory of Applied Optics, Changchun Institute of Optics, Fine Mechanics and Physics, Chinese Academy of Sciences, Changchun 130033, China
[b] Department of Electronic Information and Physics, Changzhi University, Changzhi 046011, China
[c] Key Laboratory of UV-Emitting Materials and Technology, Ministry of Education, Northeast Normal University, Changchun 130024, China

ARTICLE INFO

Keywords:
Double femtosecond lasers
Molybdenum
Nanograting structures
Surface plasmons

ABSTRACT

Femtosecond laser-induced periodic surface structures featured by a mask-free and one-step procedure provide a new fascinating prospect for the high precision manufacture applicable to diverse materials, but still face challenges in both the fabrication efficiency and the structure quality. Here, a homogenous large-area nanolithography is implemented on molybdenum surface, through using cylindrical focusing of double temporally delayed blue femtosecond lasers with orthogonal polarizations. The achieved grating structures present some unique features including the ablated narrow groove width of 100 nm, the small period of 245 nm, the smooth ridge profiles, and especially the uniform distribution in a mm-scaled range without bending, spitting and interruption. The calculated structure orientation angle shows an unprecedentedly minimum dispersion value of 5°, indicting a significant improvement on the structure uniformity compared with the observations of the single-beam femtosecond laser irradiation. The simulation results reveal that the transient spatiotemporal correlations between the localized electromagnetic field distributions from the double orthogonally polarized laser pulses constitutes a positive feedback mechanism to regularize the growth of the surface structures. A macro-sized surface pattern of such uniform structures displays good monochromatic colors and excellent broadband anti-reflection performances. This efficient laser nanolithography facilitates the applications in the fields of nanooptics.

1. Introduction

Micro or nanostructuring of solids is of significant interest because of its capability in modifying the physicochemical properties of the materials and expanding their scope of applications [1–3]. Although there exist many lithography techniques based on the photo, ion or electron beams, the fabrication of micro or nanostructures often suffers from either severe conditions or a low throughput [4–6]. Recently, an alternative convenient approach featured by a simple mask-free procedure, *i.e.*, the so-called femtosecond laser-induced periodic surface structures (fs-LIPSS), has been proved effectively for the high precision manufacture on a variety of materials [1,2,7–10], in which the structure period (Λ) can be shrunk into the near-wavelength ($\lambda > \Lambda > \lambda/2$) or even deep-subwavelength ($\Lambda < \lambda/2$) scale. Although the comprehensive understanding of the formation mechanisms is still under debate [11–12], their potential applications have already been reported in wide areas such as surface colorization [13], modification of surface wetting and tribology properties [14,15], enhancing light harvesting [16], improving biocompatibility [17], and engineering optical birefringence [18].

Currently, there are two main obstacles in the development of fs-LIPSS technology: the low efficiency for a large area of production and the irregular spatial alignment of the structures especially for the deep sub-micrometer period. The former is usually caused by the tight focusing of the laser beam through either the objective lens or spherical optical elements, thus leading to time consumption of about 10^5 min for structuring a surface area of 1 cm^2; whereas the latter is often disturbed by the bending, forking and splitting phenomena, which presents a great challenge for surface photonic device applications. To solve the first problem, S. Das, et.al demonstrated to exploit the line focus of a cylindrical lens for extended-area structuring, however the available nanostructures still remained quasi-periodic [19]. The morphological

* Corresponding author.
E-mail address: jjyang@ciomp.ac.cn (J. Yang).

https://doi.org/10.1016/j.apsusc.2021.151371
Received 1 February 2021; Received in revised form 14 September 2021; Accepted 20 September 2021
Available online 22 September 2021

regularity of fs-LIPSS is highly sensitive to both the material properties and the laser irradiation parameters. Some previous investigations demonstrated that the hard metals of W, Mo, Ti, Ni and steel are more suitable to generate the highly regular LIPSSs than the soft metals of Au, Ag, Cu and Al, due to their significant differences in the physical properties, i.e., the electron–phonon coupling coefficient, the hot electron diffusion and the melting point [20–22]. Through using either high-repetition-rate infrared femtosecond lasers (MHz, >1μm) or vacuum conditions, some authors reported to improve the spatial quality of the surface structure formation on thin metal films based on different involved mechanisms and processes such as the scanning strategy [23], the short decay length of the excited surface electromagnetic waves [24], the laser-induced oxidation [25] and the avoidance of oxidation and thermal disturbance of air plasma [26]. For the surface of bulk materials, the previous studies manifested that the structure formation can be effectively manipulated by the incident temporally shaped femtosecond laser pulses via transient dynamic processes [27–28]. In spite of these observations, femtosecond laser high-efficiency-and-quality nanostructuring of the hard metal surface, as reported here, has previously been rarely reported.

In this paper, we introduce an effective method to fabricate the large-area uniform nanostructures on hard metal of molybdenum surfaces, by cylindrical focusing of double temporally delayed blue femtosecond lasers (400 nm, 1 kHz) with orthogonal linear polarizations. At the proper ratios of the energy fluence between double laser beams, a large-area formation of the regular grating structures can be achieved, with the remarkably decreased period of about 245 nm. The uniform alignment of the surface structures was characterized by the dispersion in the structure orientation angles. The simulation of the near-field intensity distributions for the orthogonally polarized laser irradiations provides deep insights into the formation mechanisms. Further optical measurements demonstrate that such structures possess good monochromatic colors in the short-wavelength visible lights and excellent broadband antireflection performances in the wavelength range of 400–1000 nm.

2. Experimental

Fig. 1 schematically depicts an experimental setup for femtosecond laser irradiation based homogenously large-area nanoscale lithography on the metal surfaces. The employed light irradiation was a blue-colored femtosecond laser beam at the central wavelength of $\lambda = 400$ nm, which was achieved by frequency doubling of the incident infrared laser ($\lambda = 800$ nm) output from a Ti: sapphire amplifier (HP-Spitfire 50, Spectra Physics) via a beta-barium-borate (BBO) crystal. The repetition rate of the laser pulse trains was fixed at 1 kHz, with the pulse time duration of $\tau = 40$ fs and the maximum energy of $E_{max} = 7$ mJ. A spectral band-pass filter was placed after the BBO crystal to block the infrared laser components. The laser energy can be conveniently controlled by a combination of a half-wave plate with a Glan-Taylor prism. After that, through using an optical birefringent crystal of Yttrium vanadate (YVO_4), a single beam of blue femtosecond laser was split into double ones of orthogonal linear polarizations. Given by the birefringence effect for a 1.6 mm thick YVO_4 crystal, the two blue femtosecond laser beams were allowed to spatially propagate in a collinear way but with a temporal delay of 1.5 ps [29]. A ratio of energy (or fluence) between double laser beams can be varied via rotating an azimuth angle (α) of the crystal with respect to the polarization direction of the incident single-beam blue femtosecond laser. To improve the laser nanofabrication efficiency, we

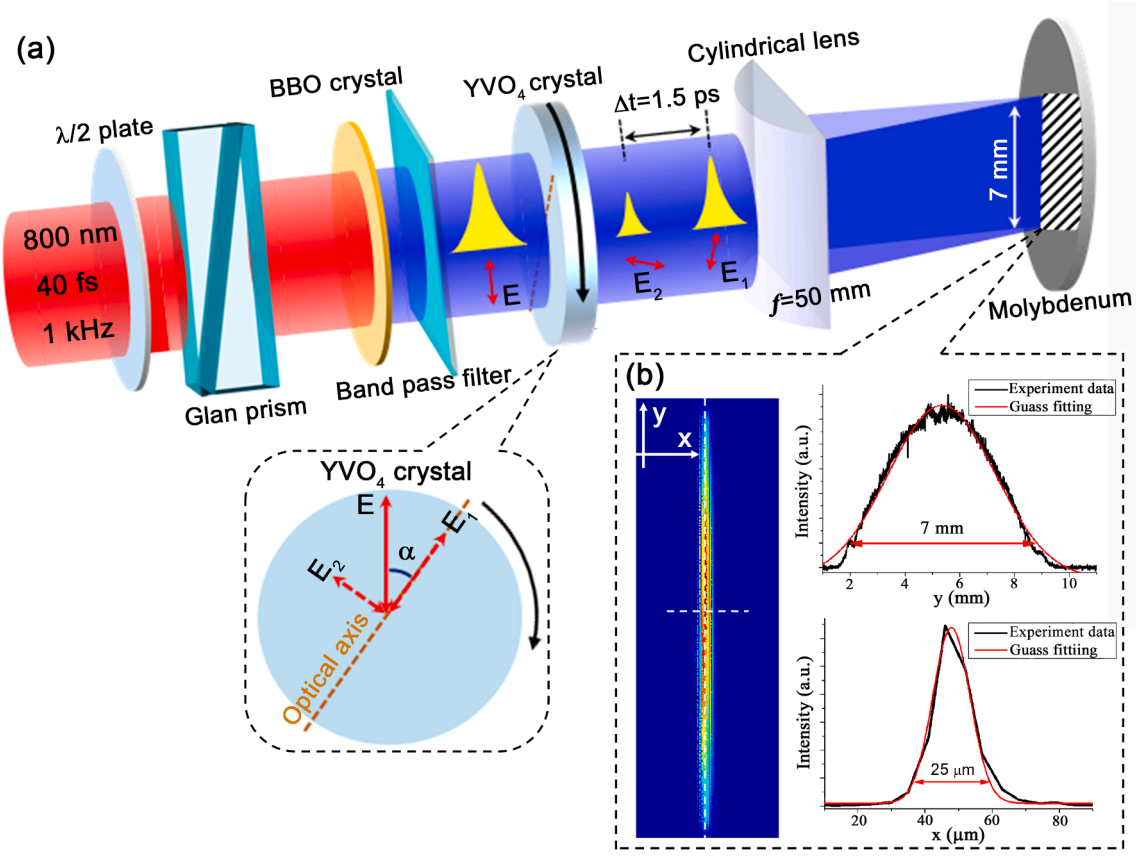

Fig. 1. (a) Sketch map of the experimental setup for the homogenous nanolithography on metal surfaces using temporally delayed blue femtosecond lasers, where double laser beams are generated via a birefringent crystal of YVO_4, and their orthogonal linear polarizations are represented by E_1 and E_2, respectively. (b) Measured line-shaped intensity distribution of the defocused spot on the sample surface and its cross-section profiles along y and x axises, respectively. Black: experimental data. Red: Gauss fitting.

adopted a cylindrical lens (with a focal length $f = 50$ mm) to give only one-dimensional confinement for the incident circular laser beam. Such cylindrically focused laser beam hitted the sample surface at normal incidence, which was placed at the position of 100 μm away before the focus for avoiding the air ionization disturbance. The measured intensity distribution of the laser beam spot on the sample using a WinCamD (LCM, DataRay) presents a line-shape with the narrowly confined dimension of approximately 25 μm and the broad unconfined dimension of approximately 7 mm at $1/e^2$ of the peak intensity, respectively, as shown in Fig. 1(b). This is in sharp contrast to the spherical focusing of the laser beam (usually down to ~ 10 μm in all dimensions) via an objective lens.

The sample material for the experiment is a mechanically polished Mo plate with a high purity (>99.98%), which is mounted on a computer controlled X-Y-Z stage (XMS-100, Newport) for the translations. Refractory metal of Mo characterized by the high elasticity modulus, low thermal expansion and high electrical conductivity, has wide applications in solar cells, microelectronics, optical elements in space, fusion reactors and gas-dynamic laser, and etc. Moreover, Mo is a preferentially selective material for producing the highly regular surface nanostructures owing to the large electron–phonon coupling coefficient, the small electron diffusion and the high melting point [20–22]. Nanostructuring of Mo will certainly improve the performance for the practical applications [30–33]. Under the fixed irradiation of femtosecond laser pulses, the sample was scanned at a velocity of $v = 0.01$ mm/s, resulting in 2500 pulses partially overlapped within each laser spot area. The calculation of the laser energy fluence on the sample surface was based on a formula of $F = 8E_0/(\pi\phi_1\phi_2)$[34], with E_0 being the pulse energy, ϕ_1 and ϕ_2 being the confined and unconfined beam dimensions, respectively. Before and after the experiments, the sample was ultrasonically cleaned in acetone solution for an hour. The surface morphologies were characterized by a scanning electron microscope (SEM, HITACI, S-4800).

3. Results and discussion

3.1. Structural morphology and characterization

In the experiment, the formation of structures on Mo surfaces was at first investigated under irradiation of the single-beam blue femtosecond laser pulses. In this case, the azimuth angle of the birefringent crystal was given as $\alpha = 0°$, thus making the blue femtosecond laser not separate into double parts even passing through the YVO_4 crystal. Accordingly, the laser-induced surface morphology is shown by SEM images in Fig. 2, where the semi-periodic grating-like structures, with orientation perpendicular to the direction of the laser polarization, are evidenced to

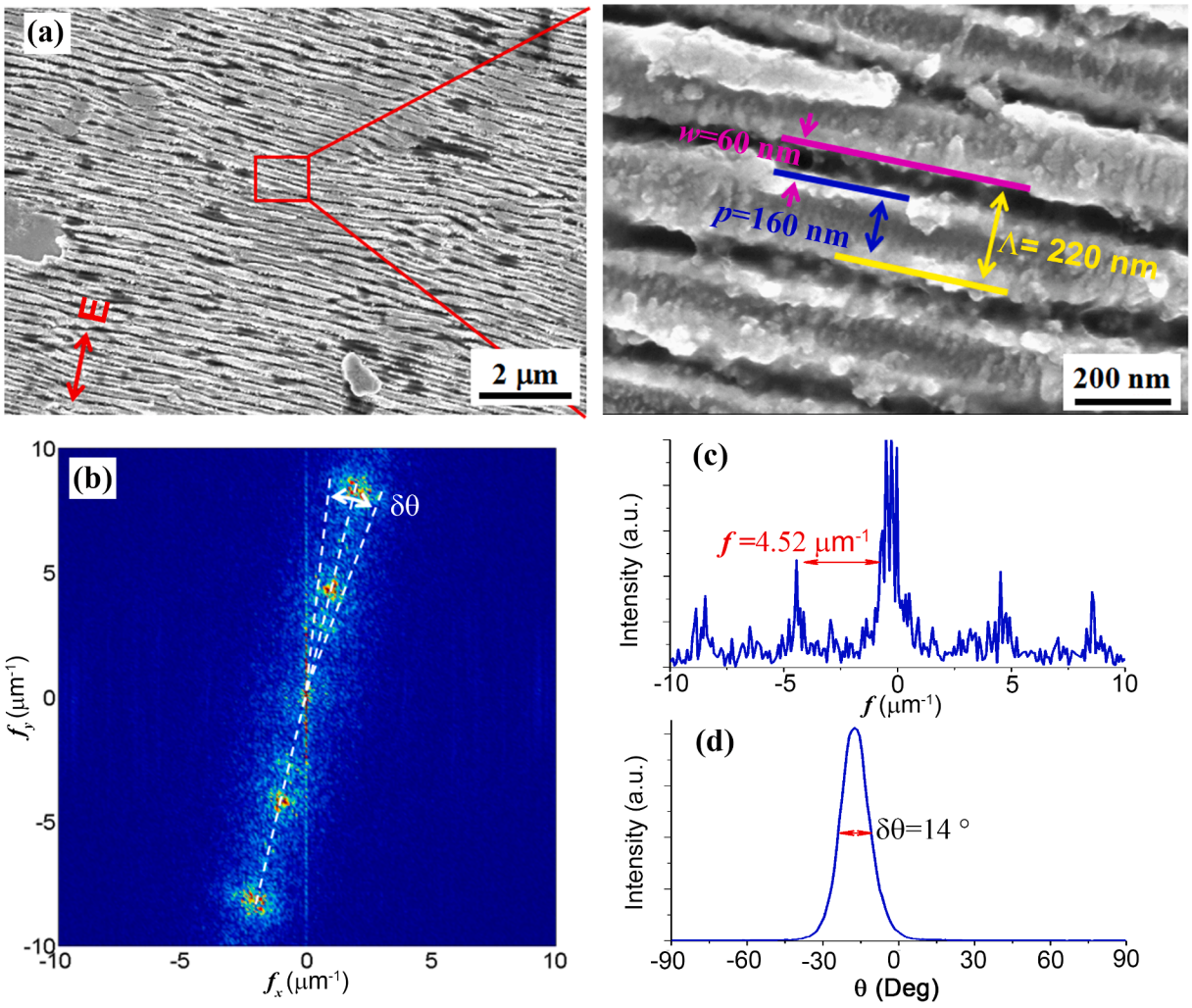

Fig. 2. Characterization of surface morphology on Mo material induced by the single-beam blue femtosecond laser irradiation at the energy fluence of F = 0.178 J/cm^2. (a) SEM images of the laser-induced surface structures, where ***E*** represents the direction of the incident laser polarization. (b) 2D-FFT image of the induced surface structures. (c) Retrieved distribution of the frequency components along the long white dot line in (b). (d) Calculated curve of the structure orientation angle distribution.

consist of bending, splitting and interruption defects, very similar to many previous observations on other material surfaces[7–8]. From the corresponding high resolution picture, we can interestingly find that both the width and spatial period of the ablative grooves were decreased to about $w = 60$ nm and $\Lambda = 220$ nm, respectively, much smaller the traditional results induced by infrared femtosecond laser pulses [15,23–24]. Fig. 2(b) illustrates a spatial frequency image of the structures obtained by two-dimensional Fast Fourier transformation (2D-FFT) method, where the calculated largely dispersive spots indicate the pronounced uncertainty of the structure alignments in the spatial domain. Especially, when the data along the chain of spots (the middle white dot line) were retrieved, as plotted in Fig. 2(c), we can find some main frequency peaks appearing on the noisy background. The measured interval of approximately $f = 4.52\ \mu m^{-1}$ between the adjacent main peaks corresponds to the reciprocal spatial period of 220 nm, in consistent with the measurement from the SEM image. According to the Ref [24], a dispersion value in the structure orientation angle (DSOA), δθ, which is defined as a full-width-at-half-maximum (FWHM) for a curve of the structure orientation angle distribution, can be used to quantitatively characterize the spatial alignment regularity of the structures. The calculation result of $\delta\theta = 14°$ in Fig. 2(d) indicates the inferior structure quality induced by the single beam of femtosecond laser pulses.

By clockwise rotating the azimuth angle of the birefringent crystal to $\alpha = 30°$, we obtained the collinear propagation of double temporally delayed blue femtosecond lasers that are linearly polarized in orthogonal directions, and the available surface structures are shown in Fig. 3 (a), wherein the laser beam E_1 arrives at the sample surface temporally ahead of the laser beam E_2, associated with the energy fluence ratio of F_1:$F_2 = 3$:1. Clearly, much different from the situations of the single laser beam irradiation, in this case the laser-induced surface structures were observed to have a dramatic improvement in the spatial alignment, *i.e.*, the ablated groove arrays are well organized within the near whole line-shaped beam spot length of 7 mm, without commonly observed defects such as bending and interruption. Moreover, orientation of such periodic surface structures is perpendicular to the polarization direction of the large-fluenced laser beam E_1. In particular, its high resolution image revealed that the grating ridges exhibit the unprecedentedly straight and smooth profiles without wavy and splitting. The surface structures were measured to have the spatial period of approximately $\Lambda = 245$ nm, associated with the groove width of as narrow as $w = 100$ nm. Because the grating ridges possess the characteristic width of only about 145 nm, they are considered to some extent as the periodic arrays of metal nanowires.

Similarly, the spatial frequency image of the surface structures can be obtained through 2D-FFT method, as shown in Fig. 3(b). Compared

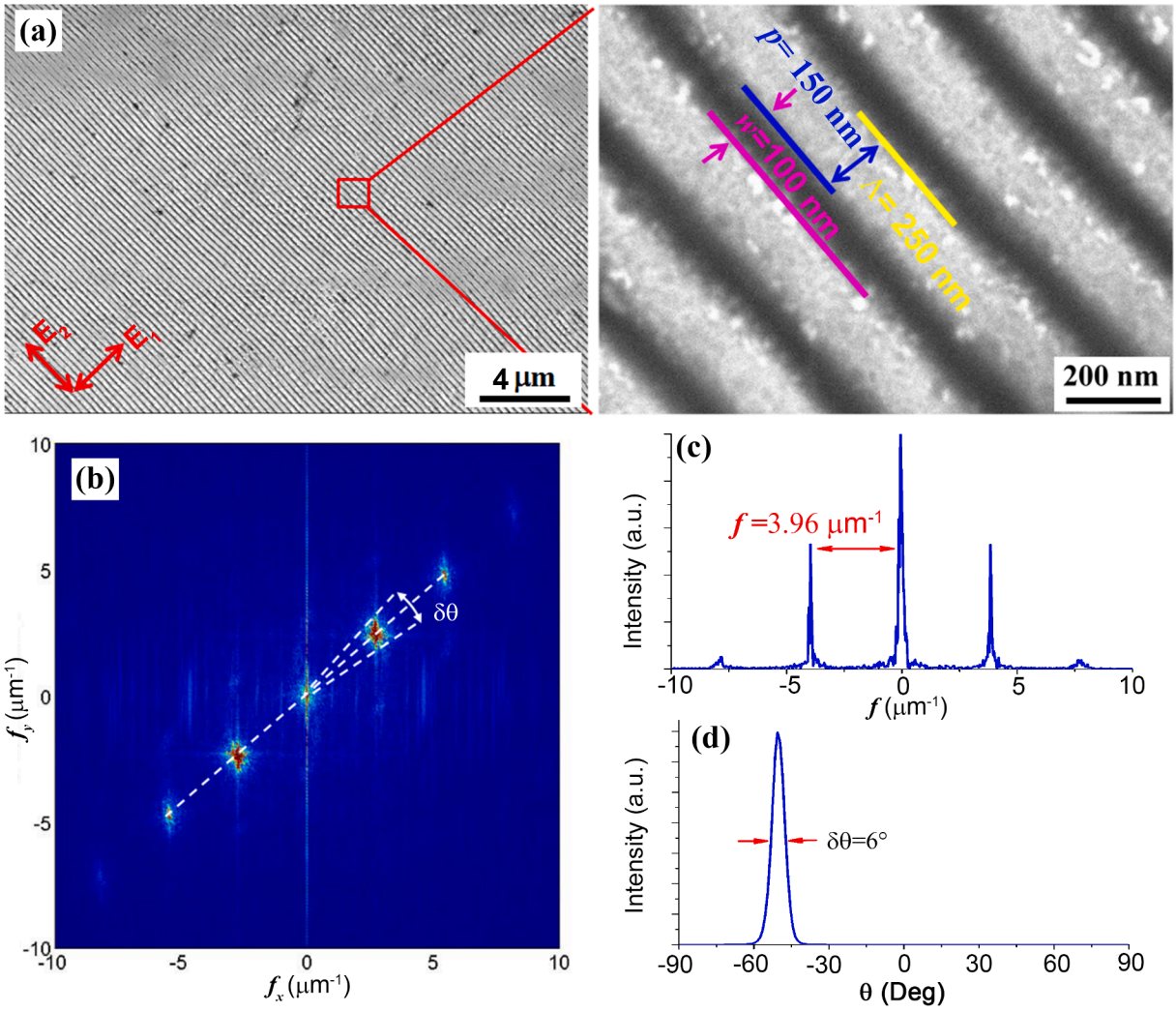

Fig. 3. Characterization of the homogenous 1D periodic grating structures on Mo surface induced by two temporally delayed blue femtosecond laser pulses with orthogonal polarizations, where the total incident laser fluence is $F = 0.178\ J/cm^2$ with the energy fluence ratio of F_1: $F_2 = 3$:1 between double laser. (a) SEM images of the laser-induced uniformly periodic surface structures. (b) 2D-FFT image of the induced surface structures. (c) Retrieved distribution of the frequency components along the long white dot line in (b). (d) Calculated curve of the structure orientation angle distribution.

with the results of the single-beam femtosecond laser irradiation, here the calculated feature size of frequency spots become much shrunk to exhibit the clear and discrete patterns rather than the galaxy connections. The retrieved data on the spot chain are shown in Fig. 3(c), in which the appearing narrow frequency peaks with the negligible noisy background implies the excellent uniformity of the structure alignment. The measured interval of $f = 3.96\ \mu m^{-1}$ between the two adjacent frequency spots suggests the reciprocal spatial period of 252 nm, in accordance with the measurement from the SEM image. Moreover, the calculated DSOA value of such surface structures, as shown in Fig. 3(e), is seen to reduce from $\delta\theta = 14^\circ$ for the case of single laser beam irradiation to $\delta\theta = 6^\circ$, indicating the significant improvement in the alignment regularity of the structures. To the best of our knowledge, the formation of such large-area uniform ablative gratings especially with the nanoscale period is unprecedented for the laser-induced surface structures.

As a matter of fact, such homogenously distributed nanograting structures can also be achieved with varying the experimental conditions. For example, Fig. 4 shows available results as the azimuth angle of the birefringent crystal rotated to $\alpha = 60^\circ$, which corresponds to the energy fluence ratio of F_1:F_2 = 1:3 between double femtosecond laser beams. In this case, although the laser-induced surface structures still present the uniform grating patterns, their spatial orientation becomes perpendicular to the direction of the linear polarization of the delayed incident laser beam E_2 with the relatively large energy fluence. Likewise the observations in Fig. 3(a), the highly regular distribution of the periodic grating structures can also take place in a mm-scaled range. From its high resolution picture, we can find that the measured spatial period of the structures is about $\Lambda = 240$ nm, associated with the groove width of about $w = 80$ nm. Furthermore, this kind of structural uniformity can be confirmed by the corresponding 2D-FFT analyses, as shown in Fig. 4 (b)-(d). Compared with the situations of $\alpha = 30^\circ$, the calculated discrete clear frequency spots turn to line up in another direction, indicating the spatial orientation of the surface structure becomes different. The measured frequency interval of $f = 4.07\ \mu m^{-1}$ suggests the average period of about 245 nm, which agrees with the measurement in the spatial domain. On the other hand, the calculation of DSOA value was decreased to $\delta\theta = 5^\circ$, indicating the remarkable homogeneity in the spatial alignment of the structures.

3.2. *Physical origins of the homogenous structure formation*

According to the previous studies[11–12], the laser-induced grating surface structures are originated from the optical interference of the laser field with the excited surface plasmon polaritons (SPPs), as shown in Fig. 5(a), which first leads to the periodic deposition of the laser energy and the subsequent selective removal of the material. In practice, the grating surface structures is formed by the multi-pulse exposure.

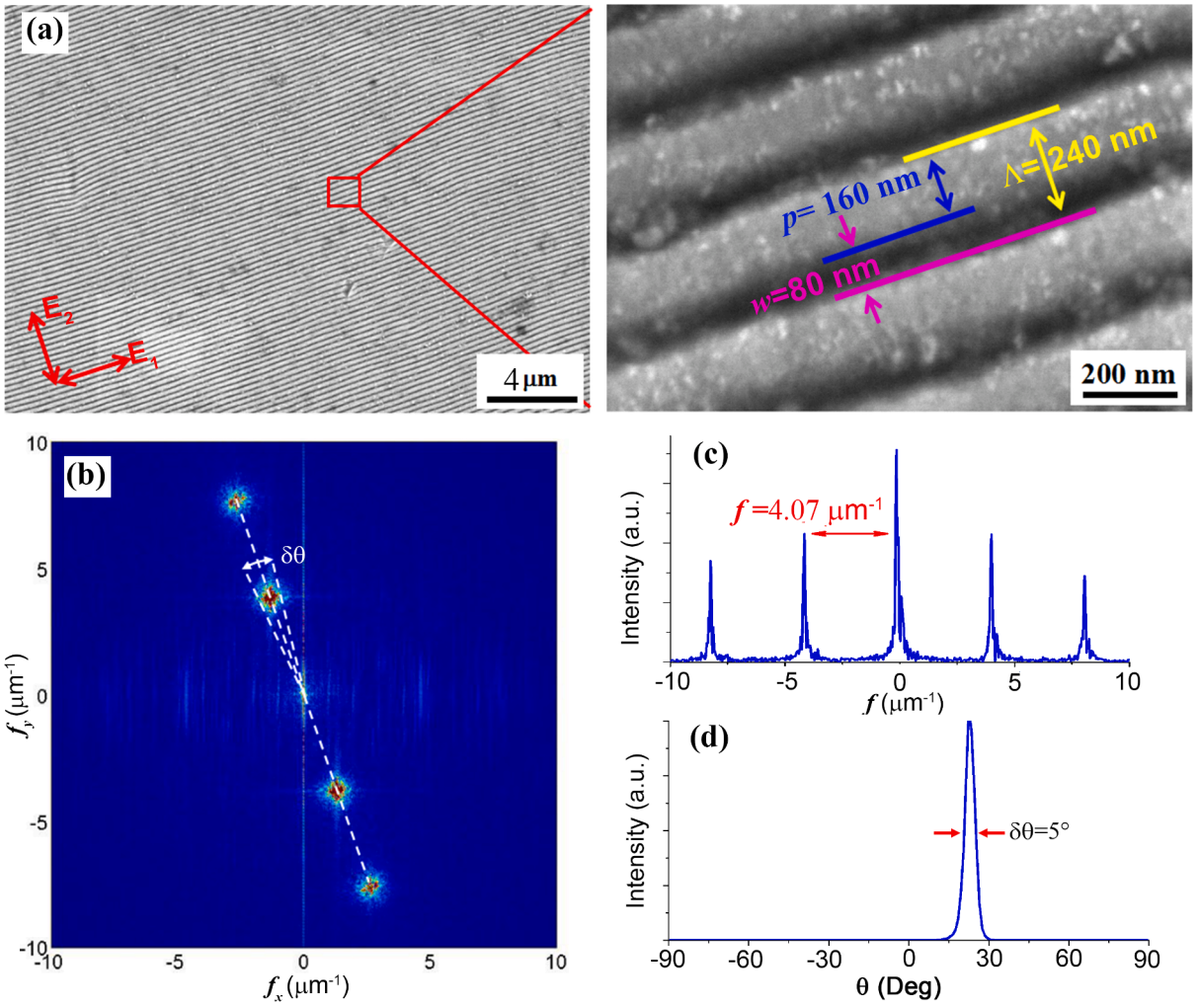

Fig. 4. Characterization of the homogenous 1D periodic grating structures on Mo surface induced by two temporally delayed blue femtosecond laser pulses with orthogonal polarizations, where the total incident laser fluence is $F = 0.178\ J/cm^2$ with the energy fluence ratio of F_1: F_2 = 1:3 between double laser. (a) SEM image of the laser-induced uniformly periodic surface structure; (b) 2D-FFT image of the induced surface structures; (c) Retrieved distribution of the frequency components along the long white dot line in (b); (d) Calculated curve of the structure orientation angle distribution.

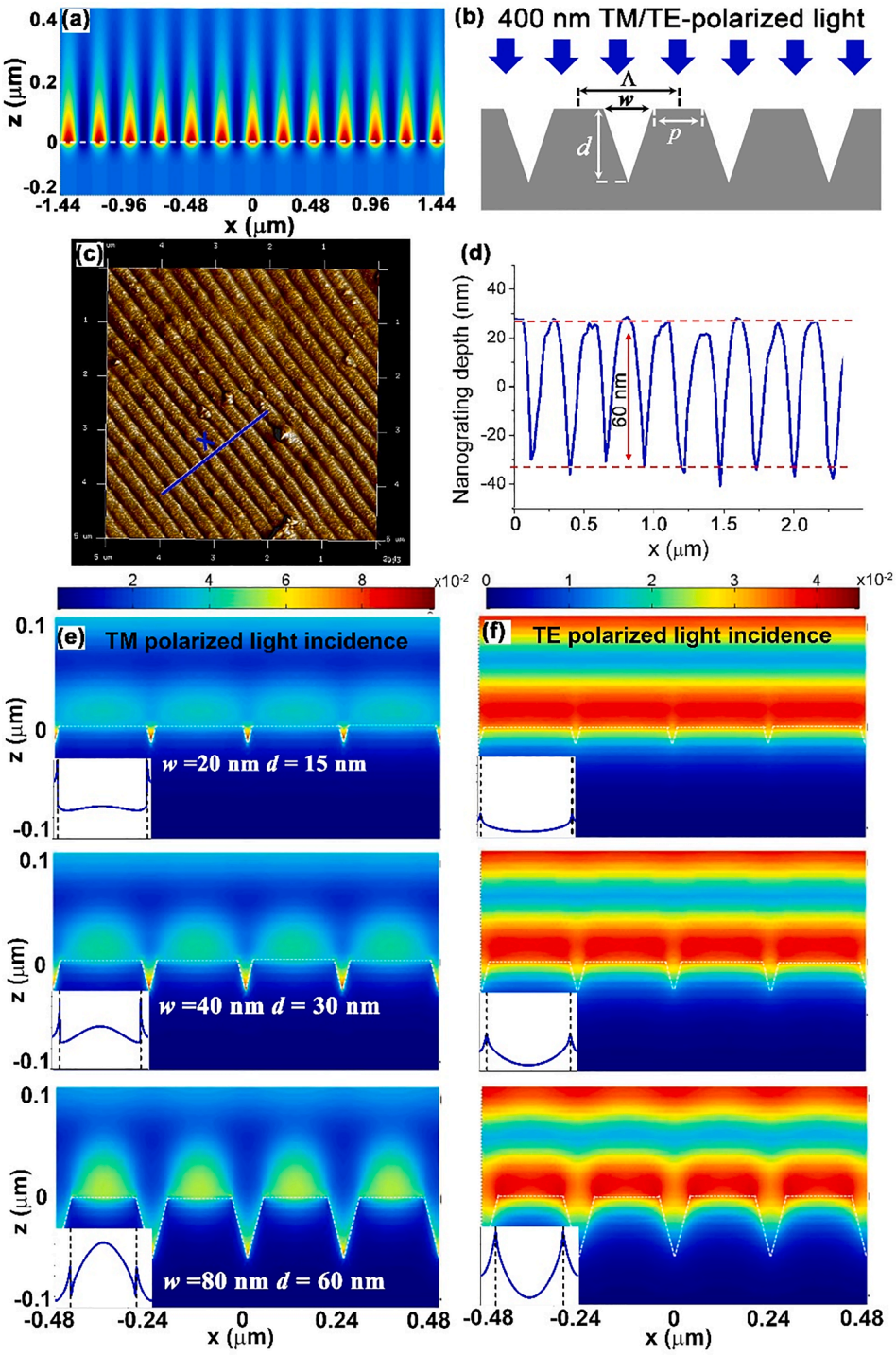

Fig. 5. Simulation of the physical processes for the periodic structure formation upon femtosecond laser irradiation at the wavelength of 400 nm. (a) Simulated SPP-based intensity fringes on the surface of Mo sample for the incident single-beam femtosecond laser. (b) A simplified structure model for the investigation of the physics for the incident double lasers with orthogonal polarizations, *i.e.*, both the transverse magnetic (TM) and transverse electric (TE) polarized lights, where Λ, *d* and *w* denote the period, depth and width of the V-shaped grooves, respectively. (c) AFM image of the laser-induced regular surface structures. (d) Measured cross-section curves along the blue line in (c). (e) Simulated spatial distributions of the electromagnetic field distribution on the V-shaped grooves with different parameters, especially when the incident light is TM polarized. The inset curves present the field distribution profiles on the transverse plane of the groove surface. (f) Simulations for the periodic structures very similar to (e), except for the incident TE polarized light.

Based on the feedback mechanisms, the laser-exposed surface morphology begins to evolve from random nanostructures into nascent periodic patterns, finally resulting in the well-aligned groove structures [1,35–36]. During these processes, the grating-assisted coupling between the laser and the excited SPPs gradually converts from a non-resonant mode into a resonant mode with the evolution of the surface morphology, which inevitably results in the local near-field enhancement on the grating ridges. This can be the basic reason for the commonly observed wavy structure appearances, especially at either the lower scanning velocities (i.e. the larger overlapped pulse numbers) or the higher incident laser fluences.

In order to have deep insights into the splitting phenomenon of the grating ridges in Fig. 2, we simulated the near-field intensity distributions on the nascent grating structures upon the single-beam femtosecond laser irradiation using the finite-difference time-domain (FDTD) method. During the simulations, the nascent grating structures were simplified into the periodic V-shaped grooves that are characterized by three structural parameters: the width of *w*, the period of *Λ*, and the depth of *d*, as shown in Fig. 5 (b). According to the experiments, the structure period was fixed as $\Lambda = 240$ nm. The permittivity of Mo target at the laser wavelength of $\lambda = 400$ nm is assumed as $\varepsilon = -1.64 + i1$ by considering the modified surface properties of the material due to the multi-pulse exposure. In this case, the incident laser light on the periodic grooves is transversely polarized (TM). For reasonably setting the

groove depth during the simulations, an AFM image of the laser-induced surface structures was measured with the cross-section profile along the direction perpendicular to the structure orientation (marked by the blue line), as shown in Fig. 5(c)-(d). It is seen that the ablated depth of the grooves approximates 60 nm.

Fig. 5(e) shows the evolution of the time-averaged Poynting vector of the electromagnetic (EM) field distribution on the V-shaped structures with different structure parameters, and the excitation of SPPs is seen clearly on the top surface of the structures, which can help to carry the EM field into the grooves. The inset curves illustrate the retrieved distribution profiles of EM field intensity on the transverse plane of the groove surface within one periodic unit. When the periodic grooves are given by the narrow width of $w = 20$ nm and the shallow depth of $d = 15$ nm, the simulated intensity of EM field is found to significantly enhance within the grooves, which consequently makes the groove further ablated in both the depth and width. For the periodic grooves with the moderate width and depth of $w = 40$ nm and $d = 30$ nm, the simulation of EM field enhancement simultaneously emerges at both the bottom and ridges of the grooves, which not only further enlarges the original grooves but also feasibly ablate traces on the grating ridges.

When the groove parameters continuously increase to $w = 80$ nm and $d = 60$ nm, the observation of EM field intensity seems to be more strengthened on the grating ridges while weakened within the grooves. Such a field distribution unavoidably results in the serious splitting of the grating ridges while almost maintaining the groove width and depth. In other words, our simulation results discover that the laser-induced surface structures have the maximum depth and width. Once these maxima reached, the subsequent laser irradiations incline to produce the splitting on the grating ridges. This is probably why the similar phenomenon was always observed in many previous reports [35–36]. Conclusively, during the multi-pulse exposure processes of the single-beam femtosecond laser irradiation, the resultant enhanced near-field laser intensity on the grating ridges is primarily responsible for the ridge splitting observations, which consequently deteriorates the spatial alignment regularity of the structures. Therefore, how to effectively avoid the ridge splitting effect is in fact crucial for the homogenous formation of the subwavelength grating structures.

When double temporally delayed femtosecond laser pulses, which possess the energy fluence ratio of approximately 3:1 or 1:3 with orthogonal linear polarizations, are employed for irradiation, a primary birthing of the periodic structures on the surface is predominated by the action of the laser pulse with relatively large energy fluence due to the higher SPP excitation. When the succeeding pulse pairs with different linear polarizations are incident on the nascent grating surface, the laser pulse with relatively large energy fluence is regarded to have the TM polarization while the laser pulse with relatively small energy fluence having the TE polarization. According to the aforementioned simulations for the single-beam laser irradiation, the incident TM-polarized laser pulse is devoted to continuous making the groove depth and width enlarge at the early stage of the structure development. Whereas for the case of incident TE-polarized laser pulse, as shown in Fig. 5(f), its excitation of SPPs is not allowed due to the lack of transverse electric fields [37], leading to no more deposition of laser energy into the nascent grooves but only field distribution within the optical penetration layer of the structure surface. The inset curves illustrate the retrieved EM field distribution profiles on the transverse plane of the groove surface within one periodic unit. Furthermore, because the incident TE-polarized light can establish the surface currents on the metal surface, more concentrations of the EM field are doomed to occur around two edges of each groove due to the air gap discontinuity [37]. With gradual increase of the groove depth and width, such local field intensity enhancement will become enlarged, which can be evidenced in inset picture of Fig. 5 (f), much different from the observations upon irradiation of the TM polarized laser.

Since the temporal delay ($\Delta t = 1.5$ ps) between the TM and TE polarized laser pulses is shorter than the relaxation time (~10 ps) of electron-lattice coupling, their dynamic processes of the energy deposition on the structures are transiently correlated in spatiotemporal domains. According to the previous studies, the incident double temporally delayed femtosecond laser pulses can promote the ablation efficiency of metallic materials via enhancing the laser energy coupling into the electron subsystem [38]. Therefore, the morphology evolution of the nascent grating structures is determined by the spatially energy depositions of both TE and TM polarized pulses and their correlation effects. In specific, at the early stage of the structure development with the smaller groove width and depth, the physical contributions of the TE-polarized laser pulse to the structure morphology can be negligible due to its insignificiant groove-edge-preference energy deposition. However, at the later stage of the structure development with the larger groove width and depth, the ridge-center-preference energy deposition of the TM light can be balanced by the groove-edge-preference energy deposition of the TE light, which finally results in a homogenous energy deposition on the structure surface. This fact not only makes the ridge splitting effectively suppressed but also allows the surface of grating structures more smooth. As a result, the positive feedbacks are constituted to regulate the growth of the nascent grating structures with multi-pulse exposures, thus finally leading to a long-range distribution of the regular structures.

3.3. Dynamic window of the structure formation

Moreover, we also carried out a lot of experiments with variable laser parameters to investigate the formation of the homogenous nanograting structures. It was found that the required scanning speeds were within a narrow range of $v = 0.01$–0.02 mm/s and the proper change for the defocusing distance of the sample surface can be $s = 50 \sim 150$ μm. With the selected parameters of $v = 0.01$ mm/s and $s = 100$ μm, we experimentally obtained the dynamic window conditions for the regular nanograting structure formation in terms of the totally incident laser fluence and the energy fluence ratio between double pulses (the first one to the second one), as illustrated in Fig. 6. Clearly, the formation of the homogenous nanograting structures is mainly concentrated within two dynamic ranges: one is featured by the laser fluence ratios of about $1{:}3 < F_1{:}\,F_2 < 1{:}2$; the other is by about $2{:}1 < F_1{:}\,F_2 < 3{:}1$. The suitable energy fluence ratio values seem to depend on the totally incident laser fluence. The lower the total incident laser fluence, the larger the suitable ratio range becomes. Otherwise, either the irregular 1D grating structures or 2D periodic structures can be observed on the sample surfaces

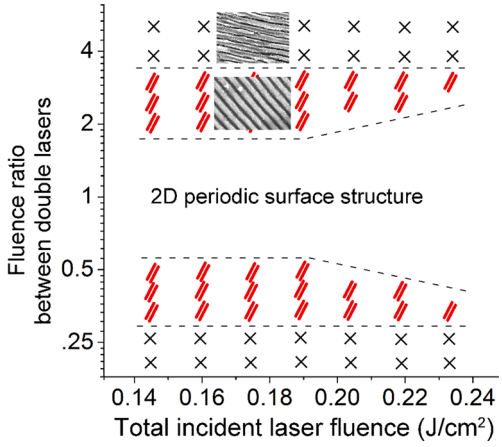

Fig. 6. Experimentally obtained a dynamic window for the homogenous nanolithography on Mo surface, in terms of the total incident laser fluence and the fluence ratio between double lasers, where the inset SEM images show the surface nanostructures with the regular and irregular profile, which are marked by the symbols of "//" and "×", respectively. The scanning speed and the defocal distance are fixed at $v = 0.01$ mm/s and $s = 100$ μm, respectively.

[39–40].

3.4. Color display and antireflection applications of the metal nanograting structures

To investigate the optical diffraction properties of such nanoscaled periodic grating structures on the metal surface, we fabricated such uniform nanograting structures into a macro-pattern of "N"-shape (with the geometric dimensions of 8 mm × 5 mm). The used experimental parameters were given by: the total laser fluence of F = 0.178 J/cm^2, the energy fluence ratio of F_1: F_2 = 1:3, the scanning speed of v = 0.01 mm/s, and the defocal distance of s = 100 μm. Thereafter, we preformed the optical diffraction of the structured patterns by placing the sample on an angular index plate, as illustrated in Fig. 7(a), where a white light source with a broad wavelength range of 400 ~ 700 nm was employed for near grazing incidence, and the diffraction signals were monitored by a fiber spectrometer. The observation (or diffraction) angle, Δϕ, describes the position of the detector with respect to the 0th order reflection light. Because the grating period is deeply less than the visible light wavelengths, here only the 1st order diffraction light of the shorter wavelengths can be observed at large angles. The measured spectra at three diffraction angles of Δϕ = 160°, 150°, 140° are shown in Fig. 7(b), whose narrow peaks with a full-width-at-half-maximum value of approximately 20 nm indicate the high monochromaticity of the color display. The measured wavelengths of three diffraction peaks are illustrated by the black dots in Fig. 7(c). The calculation of the structure periods based on the diffraction theory is shown by the blue squares in Fig. 7(c), close to the experimental measurement of Λ = 240 nm. Fig. 7(d) are the color displays of the structured surface captured by a digital camera at different observation angles, showing almost solid blue and cyan, respectively. Such vivid blue colors displayed by the metal structures have been unseen in literatures, which promises potential applications in both information displaying and ultraviolet spectroscopy.

The optical reflectivity of the structured surface was experimentally measured for both the unpolarized and the TM-polarized lights at normal incidence using a spectrometer (Ideaoptics, ARMS), respectively, as shown in Fig. 7(e). In comparison with the polished surface, the reflectivity of the structured surface demonstrates a remarkable overall drop, i.e., down to approximately 30% in the whole wavelength of 400–1000 nm for the unpolarized light, below 15 % in the wavelength range of 530–1000 nm and even below 10 % in the specific wavelength range of 615–735 nm for the TM-polarized light incidence with polarization perpendicular to the structure orientation. From these results, the excellent broadband antireflection performances are observed for both the unpolarized light and TM-polarized light, with the reflectance decrease by approximately 25% and 40%, respectively. Apart from the color display and antireflection applications, such nanostructured Mo surface can provide numerous other potential applications such as wetting modification [41], antifriction [33], antibacterial [42], and photoelectron/thermal emission enhancement [43–44].

4. Conclusions

We demonstrated an effective method for fabricating the periodic nanograting structures with large-area uniformity on hard metal surfaces, when combined the line focus of the cylindrical lens with the incident double temporally delayed blue femtosecond lasers of orthogonal polarizations. For the energy fluence ratio of R = 3:1 or 1:3 between double laser beams, the nanoscale grating structures were evidenced to uniformly distribute in a millimeter range without bending, splitting and interruption phenomena, which is in sharp contrast to the observations of the single-beam femtosecond laser irradiation. The measured spatial period of the surface structures was about 245 nm, with the narrow ablated groove width of about 100 nm. The unprecedentedly uniform alignment of the structures was identified by both the minimum DOSAs value of 5° and the clear discrete frequency spots in Fourier domain, respectively.

The formation mechanism of the laser-induced uniform surface structures was analyzed by FDTD simulations, and the correlation effect between the localized energy depositions on the nascent structure

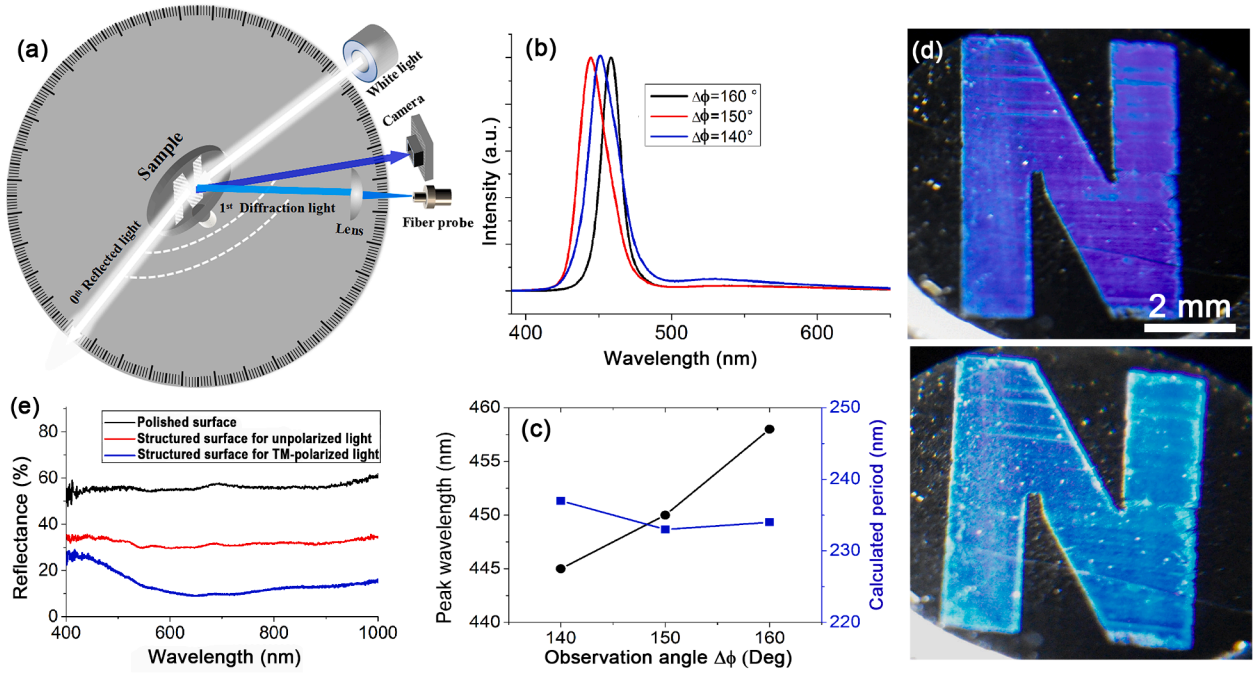

Fig. 7. Optical characterizations of the "N"-patterned metal surface consisting of the regular nanograting structures. (a) Schematic diagram of the measurement setup for optical diffraction; (b) Measured 1th order diffraction spectra at three different observation angles (Δϕ). (c) Measured diffraction peak wavelengths and calculated grating periods with varying the observation angles. (d) Structure colors of the patterned metal surface when viewed at different observation angles. (e) Measured reflectivity spectra for the unpolarized and TM-polarized lights at normal incidence. Black: polished surface. Red: structured surface for unpolarized light. Blue: structured surface for TM-polarized light.

surface from the double orthogonally polarized laser pulses was found to play an important role. In addition, the optimized laser parameters such as the scanning speed, the defocus distance, the total laser fluence and the fluence ratio was successfully established. In the optical measurements, the achieved large-area pattern of such structures displayed good monochromaticity of the structural colors for the short-wavelength visible lights and excellent broadband antireflection performances in the wavelength range of 400–1000 nm. It is believed that our investigations will benefit the generation of high efficiency and high quality nanoscale structures on the materials, which has potential applications in the surface photonic devices.

CRediT authorship contribution statement

Bo Zhao: Investigation, Writing – original draft. **Xin Zheng:** Methodology. **Yuhao Lei:** Writing – review & editing. **Hongbo Xie:** Data curation. **Tingting Zou:** Software. **Gan Yuan:** Visualization. **Wei Xin:** Writing – review & editing. **Jianjun Yang:** Conceptualization, Writing – review & editing, Funding acquisition, Project administration, Supervision.

Declaration of Competing Interest

The authors declare that they have no known competing financial interests or personal relationships that could have appeared to influence the work reported in this paper.

Acknowledgements

The work was supported by the National Natural Science Foundation of China (grant numbers 91750205, 11804334), Scientific and Technological Innovation Programs of Higher Education Institutions in Shanxi (grant number 2019L0905), the K. C. Wong Education Foundation (grant number GJTD-2018-08), and the Strategic Priority Research Program of Chinese Academy of Sciences (grant number XDA220100302).

References

[1] J. Bonse, S. Hohm, S.V. Kirner, A. Rosenfeld, J. Kruger, Laser-induced periodic surface structures - a scientifc evergreen, IEEE J. Sel. Top. Quantum Electron. 23 (2017) 9000615, https://doi.org/10.1109/JSTQE.2016.2614183.
[2] R. Buividas, M. Mikutis, S. Juodkazis, Surface and bulk structuring of materials by ripples with long and short laser pulses: Recent advances, Prog. Quant. Electron. 38 (3) (2014) 119–156, https://doi.org/10.1016/j.pquantelec.2014.03.002.
[3] Y.e. Wang, W. Liu, W. Xin, T. Zou, X. Zheng, Y. Li, X. Xie, X. Sun, W. Yu, Z. Liu, S. Chen, J. Yang, C. Guo, Back-reflected performance-enhanced flexible perovskite photodetectors through substrate texturing with femtosecond laser, ACS Appl. Mater. Interfaces 12 (23) (2020) 26614–26623, https://doi.org/10.1021/acsami.0c04124.
[4] Y. Wang, H. Hu, J. Shao, Y. Ding, Fabrication of well-defined mushroom-shaped structures for biomimetic dry adhesive by conventional photolithography and molding, ACS Appl. Mater. Interfaces 6 (4) (2014) 2213–2218, https://doi.org/10.1021/am4052393.
[5] P.G. Blauner, Focused ion beam fabrication of submicron gold structures, J. Vac. Sci. Technol. B 7 (1989) 609, https://doi.org/10.1116/1.584803.
[6] M. Imboden, D. Bishop, Top-down nanomanufacturing, Phys. Today 67 (12) (2014) 45–50, https://doi.org/10.1063/PT.3.2621.
[7] Y. Yang, J. Yang, L.u. Xue, Y. Guo, Surface patterning on periodicity of femtosecond laser-induced ripples, Appl. Phys. Lett. 97 (14) (2010) 141101, https://doi.org/10.1063/1.3495785.
[8] Y. Shimotsuma, P.G. Kazansky, J. Qiu, K. Hirao, Self-organized nanogratings in glass irradiated by ultrashort light pulses, Phys. Rev. Lett. 91 (2003) 247405, https://doi.org/10.1103/PhysRevLett.91.247405.
[9] L. Wang, Q.-D. Chen, X.-W. Cao, R. Buividas, X. Wang, S. Juodkazis, H.-B. Sun, Plasmonic nano-printing: large-area nanoscale energy deposition for efficient surface texturing, Light Sci. Appl. 6 (12) (2017) e17112, https://doi.org/10.1038/lsa:2017.112.
[10] Y. Tang, J. Yang, B. Zhao, M. Wang, X. Zhu, Control of periodic ripples growth on metals by femtosecond laser ellipticity, Opt. Express 20 (2012) 25826, https://doi.org/10.1364/OE.20.025826.
[11] J. Bonse, A. Rosenfeld, J. Krüger, On the role of surface plasmon polaritons in the formation of laser-induced periodic surface structures upon irradiation of silicon by femtosecond-laser pulses, J. Appl. Phys. 106 (10) (2009) 104910, https://doi.org/10.1063/1.3261734.
[12] M. Huang, F. Zhao, Y.a. Cheng, N. Xu, Z. Xu, Origin of Laser-induced near-subwavelength ripples: interference between surface plasmons and incident laser, ACS Nano 3 (12) (2009) 4062–4070, https://doi.org/10.1021/nn900654v.
[13] Z. Ou, M. Huang, F. Zhao, Colorizing pure copper surface by ultrafast laser-induced near-subwavelength ripples, Opt. Express 22 (2014) 17254–17265, https://doi.org/10.1364/OE.22.017254.
[14] V. Zorba, L. Persano, D. Pisignano, A. Athanassiou, E. Stratakis, R. Cingolani, P. Tzanetakis, C. Fotakis, Making silicon hydrophobic: wettability control by two-length scale simultaneous patterning with femtosecond laser irradiation, Nanotechnology 17 (13) (2006) 3234–3238, https://doi.org/10.1088/0957-4484/17/13/026.
[15] J. Bonse, R. Koter, M. Hartelt, D. Spaltmann, S. Pentzien, S. Höhm, A. Rosenfeld, J. Krüger, Femtosecond laser-induced periodic surface structures on steel and titanium alloy for tribological applications, Appl. Phys. A 117 (1) (2014) 103–110, https://doi.org/10.1007/s00339-014-8229-2.
[16] H.-C. Yuan, V.E. Yost, M.R. Page, P. Stradins, D.L. Meier, H.M. Branz, Efficient black silicon solar cell with a density-graded nanoporous surface: optical properties, performance limitations, and design rules, Appl. Phys. Lett. 95 (12) (2009) 123501, https://doi.org/10.1063/1.3231438.
[17] Y. Yang, J. Yang, C. Liang, H. Wang, X. Zhu, N. Zhang, Surface microstructuring of Ti plates by femtosecond lasers in liquid ambiences: A new approach to improving biocompatibility, Opt. Express 17 (23) (2009) 21124, https://doi.org/10.1364/OE.17.021124.
[18] G. Cheng, Q. Liu, Y. Wang, W. Zhao, G. Chen, Three-dimensional multilevel memory based on laser-polarization- dependence birefringence, Chin. Opt. Lett. 4 (2006) 111–113, https://doi.org/10.1016/S1004-9541(07)60022-6.
[19] S.K. Das, K. Dasari, A. Rosenfeld, R. Grunwald, Extended-area nanostructuring of TiO_2 with femtosecond laser pulses at 400 nm using a line focus, Nanotechnology 21 (15) (2010) 155302, https://doi.org/10.1088/0957-4484/21/15/155302.
[20] J. Wang, C. Guo, Numerical study of ultrafast dynamics of femtosecond laser-induced periodic surface structure formation on noble metals, J. Appl. Phys. 102 (5) (2007) 053522, https://doi.org/10.1063/1.2776004.
[21] K.e. Cheng, K. Cao, Y. Zhang, R. Han, D. Feng, J. Liu, S. Zhang, Z. Sun, T. Jia, Ultrafast dynamics of subwavelength periodic ripples induced by single femtosecond pulse: from noble to common metals, J. Phys. D: Appl. Phys. 53 (28) (2020) 285102, https://doi.org/10.1088/1361-6463/ab82d9.
[22] S. Sakabe, M. Hashida, S. Tokita, Y. Miyasaka, M. Shimizu, S. Inoue, in: Scaling of grating spacing with femtosecond laser fluence for self-organized periodic structures on metal, Progress in Nonlinear Nano-Optics. Nano-Optics and Nanophotonics. Springer, Cham, 2015, pp. 103–115, https://doi.org/10.1007/978-3-319-12217-5_6.
[23] A. Ruiz de la Cruz, R. Lahoz, J. Siegel, G.F. de la Fuente, J. Solis, High speed inscription of uniform, large-area laser-induced periodic surface structures in Cr films using a high repetition rate fs laser, Opt. Lett. 39 (8) (2014) 2491, https://doi.org/10.1364/OL.39.002491.
[24] I. Gnilitskyi, J.Y. Derrien, Y. Levy, N.M. Bulgakova, M. Tomá, L. Orazi, High-speed manufacturing of highly regular femtosecond laser-induced periodic surface structures: physical origin of regularity, Sci. Rep. 7 (2017) 8485, https://doi.org/10.1038/s41598-017-08788-z.
[25] B. Öktem, I. Pavlov, S. Ilday, H. Kalaycıoğlu, A. Rybak, S. Yavaş, M. Erdoğan, F.Ö. Ilday, Nonlinear laser lithography for indefinitely large area nanostructuring with femtosecond pulses, Nat. Photon. 7 (2013) 897–901, https://doi.org/10.1038/NPHOTON.2013.272.
[26] F. Wang, B.o. Zhao, Y. Lei, J. Yang, C. Guo, Producing anomalous uniform periodic nanostructures on Cr thin films by femtosecond laser irradiation in vacuum, Opt. Lett. 45 (6) (2020) 1301, https://doi.org/10.1364/OL.382322.
[27] W. He, J. Yang, C. Guo, Controlling periodic ripple microstructure formation on 4H-SiC crystal with three time-delayed femtosecond laser beams of different linear polarizations, Opt. Express 25 (2017) 5156–5168, https://doi.org/10.1364/OE.25.005156.
[28] G. Giannuzzi, C. Gaudiuso, C.D. Franco, G. Scamarcio, P.M. Lugarà, A. Ancona, Large area laser-induced periodic surface structures on steel by bursts of femtosecond pulses with picosecond delays, Opt. Laser. Eng. 114 (2019) 15–21, https://doi.org/10.1016/j.optlaseng.2018.10.006.
[29] B. Dromey, M. Zepf, M. Landreman, K. O'Keeffe, T. Robinson, S.M. Hooker, Generation of a train of ultrashort pulses from a compact birefringent crystal array, Appl. Opt. 46 (2007) 5142–5146, https://doi.org/10.1364/AO.46.005142.
[30] A.K. Sharma, J. Smedley, T. Tsang, T. Rao, Formation of subwavelength grating on molybdenum mirrors using a femtosecond Ti:sapphire laser system operating at 10 Hz, Rev. Sci. Instrum. 82 (3) (2011) 033113, https://doi.org/10.1063/1.3569763.
[31] X. Hu, W. Zhang, X. Liu, Y. Mei, Y. Huang, Nanostructured Mo-based electrode materials for electrochemical energy storage, Chem. Soc. Rev. 44 (8) (2015) 2376–2404, https://doi.org/10.1039/C4CS00350K.
[32] L. Kotsedi, P. Mthunzi, Z.Y. Nuru, S.M. Eaton, P. Sechoghela, N. Mongwaketsi, R. Ramponi, M. Maaza, Ramponi MMaaza, Femtosecond laser surface structuring of molybdenum thin films, Appl. Surf. Sci. 353 (2015) 1334–1341, https://doi.org/10.1016/j.apsusc.2015.08.047.
[33] A. Voznesenskaya, D. Kochuev, A. Zhdanov, Research on the tribological properties of periodic micro- and nanostructures on the molybdenum surface obtained as a result of laser action, Mater. Today Proc. 19 (2019) 1–4, https://doi.org/10.1016/j.matpr.2019.07.069.
[34] J. Bonse, S. Gräf, Maxwell meets marangoni—a review of theories on laser-induced periodic surface structures, Laser Photonics Rev. 14 (10) (2020) 2000215, https://doi.org/10.1002/lpor.202000215.

[35] M. Huang, Y. Cheng, F. Zhao, Z. Xu, The significant role of plasmonic effects in femtosecond laser-induced grating fabrication on the nanoscale, Ann Phys-Berlin 525 (2013) 74–86, https://doi.org/10.1002/andp.201200136.
[36] J.-W. Yao, C.-Y. Zhang, H.-Y. Liu, Q.-F. Dai, L.-J. Wu, S. Lan, A.V. Gopal, V. A. Trofimov, T.M. Lysak, High spatial frequency periodic structures induced on metal surface by femtosecond laser pulses, Opt. Express 20 (2) (2012) 905, https://doi.org/10.1364/OE.20.000905.
[37] Y. Xie, A.R. Zakharian, J.V. Moloney, M. Mansuripur, Transmission of light through slit apertures in metallic films, Opt. Express 12 (2004) 6106–6121, https://doi.org/10.1364/OPEX.12.006106.
[38] G. Du, Q. Yang, F. Chen, Y. Ou, Y. Wu, X. Hou, Ultrafast dynamics of laser thermal excitation in gold film triggered by temporally shaped double pulses, Int. J. Therm. Sci. 90 (2015) 197–202, https://doi.org/10.1016/j.ijthermalsci.2014.12.011.
[39] H. Qiao, J. Yang, F. Wang, Y. Yang, J. Sun, Femtosecond laser direct writing of large-area two-dimensional metallic photonic crystal structures on tungsten surfaces, Opt. Express 23 (2015) 26617–26627, https://doi.org/10.1364/OE.23.026617.
[40] X. Zheng, B.o. Zhao, J. Yang, Y. Lei, T. Zou, C. Guo, Noncollinear excitation of surface plasmons for triangular structure formation on Cr surfaces by femtosecond lasers, Appl. Surf. Sci. 507 (2020) 144932, https://doi.org/10.1016/j.apsusc.2019.144932.
[41] M. Hishiki, X. Yu, M. Sudo, F. Itoigawa, S. Ono, Fabricating fine structures induced by femtosecond laser on molybdenum surface, in: 2018 Conference on Lasers and Electro-Optics Pacific Rim (CLEO-PR), 2018, pp. 1–2.
[42] S.A. Jalil, M. Akram, J.A. Bhat, J.J. Hayes, S.C. Singh, M. ElKabbash, C. Guo, Creating superhydrophobic and antibacterial surfaces on gold by femtosecond laser pulses, Appl. Surf. Sci. 506 (2020) 144952, https://doi.org/10.1016/j.apsusc.2019.144952.
[43] T.Y. Hwang, A.Y. Vorobyev, C. Guo, Surface-plasmon-enhanced photoelectron emission from nanostructure-covered periodic grooves on metals, Phys. Rev. B 79 (2009) 085425, https://doi.org/10.1103/PhysRevB.79.085425.
[44] A.Y. Vorobyev, V.S. Makin, C. Guo, Brighter light sources from black metal: significant increase in emission efficiency of incandescent light sources, Phys. Rev. Lett. 102 (2009) 234301, https://doi.org/10.1103/PhysRevLett.102.234301.